Netting Crystal Nuclei in Metal–Organic Framework Cavities

Alan Braschinsky, Toby J. Blundell, and Jonathan W. Steed*

Nucleation plays an important role in crystallization outcomes, but it is still poorly understood because it occurs on short timescales and small size scales. Consequently, nucleation mechanisms are still challenging to comprehend and predict. Gaining a better understanding, and potentially control, over nucleation pathways, can significantly aid toward more consistent and targeted crystallization outcomes. To achieve this, facile methods that allow for an accurate depiction and analysis of nucleus-sized clusters are needed. Herein, the use of crystalline metal–organic frameworks (MOFs) is reported to entrap clusters of small organic molecules, allowing for an accurate representation of the size and shape of the confined clusters via single-crystal X-Ray diffraction analysis. This is realized by synthesizing high-quality single crystals of lanthanum-based MOFs, which provides well-defined pore spaces for the encapsulation of guest molecules. The results show that the size and shape of the guest molecular clusters within MOFs significantly differ from their bulk equivalents, suggesting that this method can also be used toward discovering novel polymorphs. Additionally, the findings indicate that these small molecular clusters form via intermolecular interactions that do not always dominate the bulk packing, shedding new light on the initial molecular aggregation mechanisms of precritical nuclei.

1. Introduction

Crystallization is a process of fundamental importance in the chemical, food, and pharmaceutical industries. The nucleation process is pivotal for the formation of crystalline materials, impacting properties such as morphology, polymorphism, and particle size, but remains poorly understood due to difficulties in studying subcritical molecular clusters. Classical and nonclassical theories have been proposed to explain nucleation mechanisms, but structural insight is lacking because nuclei exist in an intermediate size regime between the size of individual molecules and bulk materials.[1–3] Confinement chemistry has become an increasingly relevant field because nanoconfined materials can exhibit unique physicochemical and magnetic properties as compared to their bulk.[4,5] Understanding nucleation under confinement can reveal unique properties and help design better matrices for targeted crystallization outcomes. Confinement can be used to observe various stages of the crystallization processes, as demonstrated by Mollica and co-workers in 2021.[6] The authors utilized dynamic nuclear polarization (DNP)-enhanced NMR spectroscopy to investigate crystallization processes of glycine within the nanometric pores (7–8 nm) of SBA-15 silica material. The enhanced NMR sensitivity enabled by DNP allows the detection of intermediate phases during the crystallization process, and the crystallization processes of glycine are shown to evolve slower as compared to the bulk material. Overall, these insights provide a better understanding of crystallization processes under confinement and are a highlight of important advances made in the field so far. Still, there is a lack of understanding of the molecular aggregation mechanisms that guide the nucleation pathways on the nanoscale.

Single-crystal-to-single-crystal (SCSC) transitions are a class of solid-state reactions in which a single crystal undergoes a change in its chemical composition resulting in a product while retaining its single crystallinity.[7–9] Solid-state transformations are undertaken by applying an external stimulus to the target crystal which commonly exhibits a change in its physicochemical properties, such as magnetism, porosity, or chirality, after the transition.[10,11] In many cases, single crystallinity is lost during these solid-state transformations.[12] However, if high crystallinity can be retained giving an SCSC transition, single-crystal diffraction analysis allows direct determination of the molecular structures of the new material. Owing to their crystallinity and porosity, metal–organic frameworks (MOFs) have been employed in a confinement context as crystalline sponges, a method developed by Fujita and co-workers in 2013 which utilizes a SCSC transition within the pores of a single crystal of a MOF, as a way to determine the molecular structures of difficult-to-crystallize materials encapsulated inside the pores of MOF single crystals.[13,14] The method involves soaking a single crystal of a MOF inside a solution containing the desired guest which diffuses into the cavities of the framework.[15] Single-crystal structure determination on the resulting MOF

A. Braschinsky, T. J. Blundell, J. W. Steed
Department of Chemistry
Durham University
South Road, Durham DH1 3LE, UK
E-mail: jon.steed@durham.ac.uk

The ORCID identification number(s) for the author(s) of this article can be found under https://doi.org/10.1002/sstr.202400300.

crystal subsequently results in the determination of the structure of the included guest molecule. Crystalline sponge methods, however, focus on molecular structure, rather than the crystal structure of guest molecule aggregates.

In the context of confinement of molecular aggregates, however, MOFs are potentially highly useful. First, they are capable of confining a wide range of compounds inside their tunable pores and second, they offer a way to crystallographically isolate and structurally characterize the shape, size, and packing arrangement of encapsulated aggregates and compare their structural and physicochemical properties to the bulk. For instance, Long and co-workers have reported precise control over the shape and size of metal halide sheets grown in the pores of a bipyridine-based MOF.[10] Additionally, Eddaoudi and co-workers have reported a cluster of 114 water molecules in a cubic cage of a MOF.[16] Such large aggregates approach the size of critical nuclei. For example, a study of ice nucleation based on observing the crystallization temperatures of materials within microemulsions followed by measurement of the microemulsion droplet size suggests that the critical nucleus contains 70-210 water molecules for pool radii of ≈ 1.2–1.8 nm.[17] For molecular compounds, the critical nucleus size can be significantly smaller, e.g., 5–50, for typical crystallization conditions of several proteins.[18] Herein, we present the synthesis, structure, and guest cluster exchange properties of mesoporous lanthanoid MOFs able to capture meaningfully large clusters of small molecules (CCM-1 and CCM-2, respectively) and demonstrate their ability to entrap arrays of molecular guests and undergo exchange of subcritical nucleus-sized molecular clusters in the solid state.

2. Results and Discussion

2.1. Structure and Characterization of MOFs

In 2008, a series of isomorphous lanthanide MOFs based on 4,4′-biphenyldicarboxylic acid (H$_2$BPDC) as the organic linker were reported by You and co-workers.[19] Among the lanthanides used to synthesize these MOFs were europium(III), samarium(III), lanthanum(III), cerium(III), gadolinium(III), and neodymium(III). In 2012, the same neodymium-based MOF reported by You and co-workers was also published by Łyszczek and Mazur with the only difference being the nature of the encapsulated solvent.[20] In addition, a praseodymium(III)-based isomorphous framework was also synthesized by Sessler and co-workers in 2016.[21] As these MOFs contain well-defined mesopores and exhibit high crystallinity, we aimed to apply these materials for use as crystalline confining matrices. These materials are also of interest because they contain accessible metal coordination sites that can serve to anchor guest molecules within the pores.

The synthesis of these MOFs was undertaken using the solvothermal method. A dimethyl formamide (DMF) solution containing a 1:1 ratio of lanthanum(III) nitrate hexahydrate and H$_2$BPDC metal-to-ligand was made up into a Teflon-lined acid digestion vessel, which was subsequently placed in an isothermal oven and heated at 120 °C for 72 h (**Scheme 1**) resulting in the crystallization of transparent plank-shaped single crystals termed of the lanthanum-based MOF, herein termed CCM-1 (**C**luster **C**apturing **M**etal–organic-framework-**1**). Analogous reactions with europium(III) chloride hexahydrate, cerium(III) nitrate hexahydrate, and praseodymium(III) nitrate hexahydrate resulted in isomorphous MOFs, termed CCM-2-4, respectively. The synthesis of CCM-1 MOF was performed with trifluoroacetic acid (TFA) as a modulator[22] while the syntheses of CCM-2–4 MOFs were performed without the presence of TFA.

Figure 1a shows the IR spectra of MOFs CCM-1–4, along with the organic linker H$_2$BPDC. In each of the CCM-series MOFs, the broadband corresponding to the O—H stretching of the carboxylic acid (3055–2547 cm^{-1}, purple trace) is not present, indicating its deprotonation as a result of coordination to the lanthanoid metal centers. The C—H stretching (2929 and 2864 cm^{-1} shown for CCM-1) of the DMF molecules inside the pores of the MOFs appears for all CCM-series MOFs. Additionally, the band at 1669 cm^{-1} corresponding to the asymmetric C=O stretching of the H$_2$BPDC linker is replaced with a wider band centered at 1654 cm^{-1} corresponding to both coordinated and noncoordinated DMF molecules inside the pores of the frameworks.[23] Figure 1b shows the experimental and simulated powder X-ray diffraction (PXRD) traces of the as-synthesized MOFs. The similarities in the experimental powder patterns of CCM-1–4 MOFs indicate that they possess very similar unit cells and are likely isostructural. Additionally, very good agreement between the simulated and experimental traces also indicates high bulk purity. There are, however, differences in the low-angle peaks between the simulated and experimental PXRD patterns of the CCM-MOFs as a result of the crystals' plank-shaped morphology leading to preferred orientation. Thermogravimetric analysis performed on the CCM-1–4 crystals shows that each framework is stable up to 400 °C (Figure S1, Supporting Information).

Low-temperature (120 K) single-crystal X-Ray diffraction (SC-XRD) analysis reveals that the crystals from the reaction containing lanthanum(III) comprise the previously reported mesoporous MOF framework with the formula La(BPDC)$_{1.5}$(DMF)$_3$ (CCM-1). CCM-1 crystallizes in the Sohncke space group C2 implying a chiral packing arrangement despite the achiral nature of the components, making it a potentially attractive MOF for enantioselective applications.[24] **Figure 2**a shows the structure of CCM-1 along the crystallographic c axis. The framework consists of lanthanum(III) metal centers octa-coordinated in a square antiprismatic coordination geometry to six BPDC^{2-}
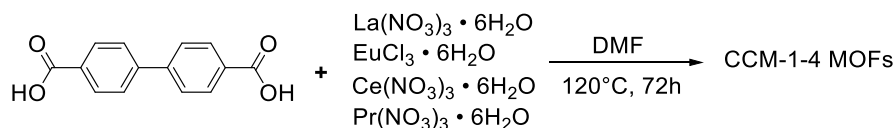
Scheme 1. General synthetic procedure for the preparation of CCM-1–4 MOFs.
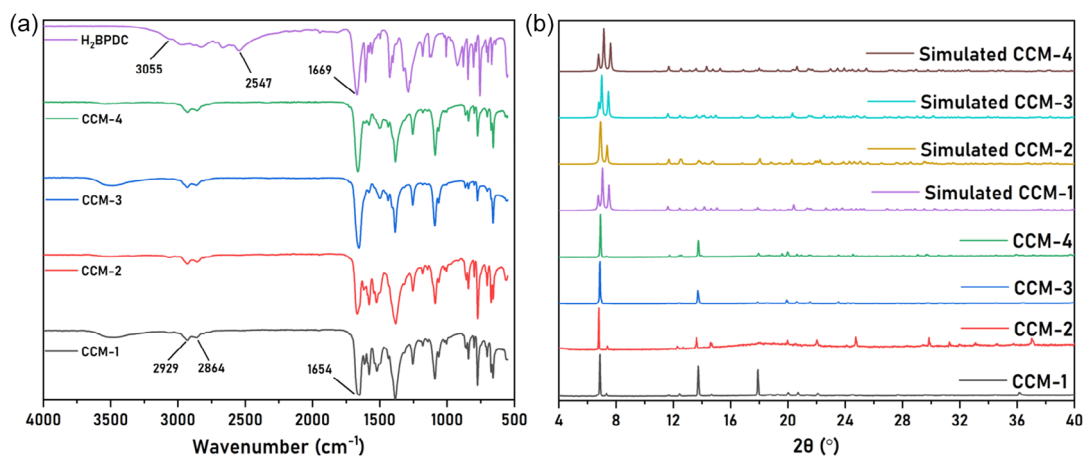
Figure 1. a) FT-IR spectra of the as-synthesized MOFs and the organic linker H_2BPDC. b) Experimental and simulated PXRD traces of MOFs CCM-1–4. Simulated patterns derived from single-crystal data.
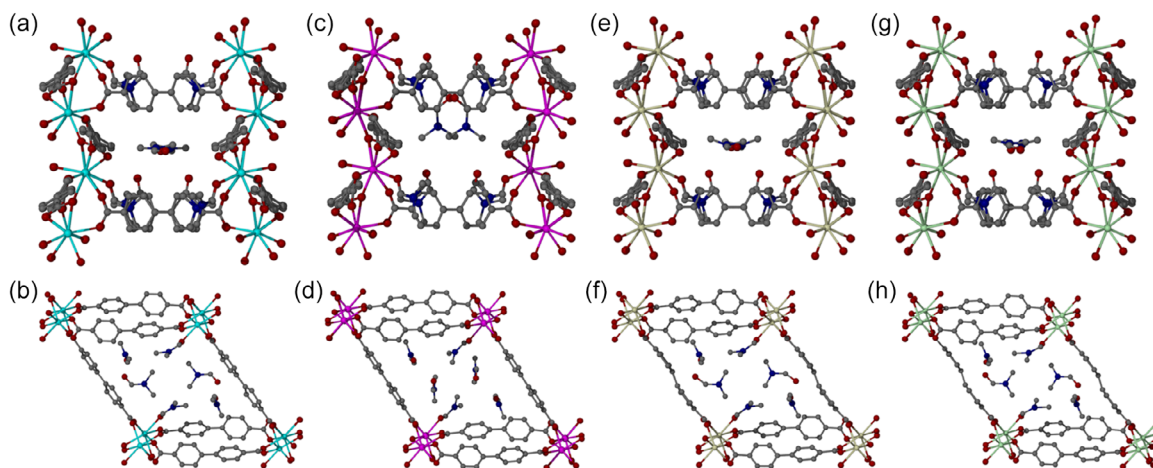
Figure 2. SC-XRD structures a,b) CCM-1, c,d) CCM-2, e,f) CCM-3, and g,h) CCM-4. Top and bottom rows depict the crystallographic c and b axes, respectively. Gray: C. Blue: N. Red: O. Light blue: La. Pink: Eu. Beige: Ce. Light green: Pr. Hydrogen atoms omitted for clarity.

ligands and one DMF solvent molecule. The secondary building units (SBUs) form metal nodes connected to each other in a zigzag chain, a common phenomenon for rare-earth MOFs assembled by carboxylic acid organic linkers.[25,26] Figure 2b shows the view along the crystallographic b axis displaying the rhombic pores. Due to the rod-shaped connection of the metal centers, two types of channel pores exist with cross section 15.0×26.4 Å and 12.4×26.0 Å. While there are slight differences, these pore channel sizes are nearly identical in all of the CCM-series MOFs. The pore volume of CCM-1 was determined by using the void analysis tool in Mercury 4.0,[27] using a probe radius of 1.2 Å, of CCM-1 is 1608 Å^3 (51.1% of the unit cell).

MOFs isostructural to CCM-1 were synthesized with europium(III), cerium(III), and praseodymium(III) metal centers, termed CCM-2–4, respectively. Efforts were made to also crystallize the gadolinium(III)-based MOF counterpart, but single crystals were not obtained from this reaction. Single crystals of CCM-2, similar to CCM-1, are transparent but emit a pinkish luminescence under UV light (Figure S3b, Supporting Information), distinctive to europium-based materials.[28] Meanwhile, single crystals of CCM-3 and CCM-4 exhibit a green color. As expected, the CCM-1–4 MOFs mainly differ from each other by the M–L coordination bond lengths and the slight variance in their pore sizes. The coordination bond lengths in CCM-2 are shorter than those in CCM-1 due to a smaller ionic radius of europium(III).[29] The Ln—O bond lengths range from $2.416(4)–2.710(4)$ Å and $2.322(4)–2.647(4)$ Å for CCM-1 and CCM-2, respectively. The Ce—O bond lengths in CCM-3 range from $2.385(6)$ to $2.683(5)$ Å, in between CCM-1 and CCM-2 as the ionic radius of cerium(III) is in between that of lanthanum(III) and europium(III).2322 Finally, the bond lengths in CCM-4 range from $2.373(4)$ to $2.703(4)$ Å. The main difference in the frameworks is the orientation of the BPDC^{2-} linkers in CCM-3 and CCM-4 compared to CCM-1 and CCM-2. In the former, the linkers are slightly bent (Figure 2f,h) as opposed to being relatively directly aligned between the metal centers as they are in CCM-1 and CCM-2 (Figure 2b,d). This indicates that the CCM-series MOFs are capable of exhibiting some structural

**ADVANCED
SCIENCE NEWS**

www.advancedsciencenews.com

**small
structures**

www.small-structures.com

flexibility which can aid in encapsulating guest molecules with different geometries. The underlying topology of all frameworks is best described using the **tsy** topology, a 3-nodal and $4^2,6$-coordinated, net (Figure S2, Supporting Information) as determined by ToposPro.[30] This is not an uncommon topology and the Cambridge Structural Database[31] (CSD) contains 86 structures that exhibit the **tsy** topology.

2.2. Analysis of Solvent Clusters in CCM-MOFs

The capability of analyzing single-crystal structures of guest molecules inside the CCM-series MOFs can lead to insights into how packing arrangement of materials changes when removed from conventional crystallization conditions. The DMF clusters in CCM-1, CCM-3, and CCM-4 are nearly identical, and only in CCM-2 there is a slight difference. In the pores of the latter, the solvent dimers are disordered and can be modeled to be perpendicular (as in CCM-1, 3, and 4 MOFs) or oriented along the pore as shown in Figure 2d. Even though the MOF frameworks exhibit nearly identical structures, the packing of DMF molecular clusters in CCM-1 and CCM-2 differs slightly. Inside both pores, DMF forms hexamers in 4–2–4–2 repeating layers. In CCM-1, DMF dimers are oriented in a perpendicular fashion to the tetramers, i.e., along the c axis pore (Figure 2a,b). However, in CCM-2 the solvent dimers are disordered and can be modeled to point along the b axis pore or perpendicularly to the tetramer. In this case, the former is shown as this way the encapsulated DMF molecules form a more discrete hexamer as compared to the DMF cluster in CCM-1. You and co-workers report only one DMF molecule per asymmetric unit for every reported MOF, suggesting that the other DMF molecules were too severely disordered for accurate crystallographic description.[19] On the other hand, Sessler and co-workers were able to crystallographically determine the tetramers similar to those in CCM-1–4 MOFs while the dimers were not modeled, likely due to the severe disorder.[21] In the crystal structure of CCM-1, no formyl hydrogen atoms participate in hydrogen bonding with either the framework or solvent molecules. On the other hand, in CCM-2 the encapsulated DMF molecules participate in hydrogen bonding with the MOF framework. In particular, a C···O distance of 3.373(6) Å between a DMF and the framework is observed, while the same oxygen atom also partakes in another weak intermolecular hydrogen bond interaction, 3.387(13) Å, with a neighboring DMF methyl hydrogen atom (**Figure 3**a, red dashed line).

Bulk DMF is known to crystallize in one polymorphic form containing dimeric and tetrameric hydrogen bonded rings, as shown in Figure 3b.[32] One of two formyl hydrogen atoms is involved in hydrogen bonding with the oxygen atom of the formyl C=O while other hydrogen bonding interactions form between the methyl hydrogen atoms and the two formyl C=O moieties. The single-crystal structures of CCM-1 and CCM-2 show that the asymmetric unit of each MOF contains three symmetry-independent DMF molecules which make up groups of hexamers along the cavity of the pore. In fact, hexamers are also observed in CCM-1–4 MOFs (Figure 2b,d,f,h, respectively) and similar to bulk DMF also consists of dimers that are a part of hexamers.[32,33] However, DMF encapsulated in CCM MOFs does not form any hydrogen bonded clusters in contrast to the bulk behavior. This could be due to the weak nature of the DMF intermolecular hydrogen bonds which are not strong enough to add directionality to the encapsulated DMF clusters.

The direct guest exchange capabilities of CCMs were tested with small molecule solvents as target guests. Single crystals of MOFs were soaked in a range of potential guest solvents at room temperature. Within 24 h crystallinity is lost or the CCM crystals become cracked in most solvents, with the exception of dimethyl sulfoxide (DMSO). The fourier transform infrared (FT-IR) spectrum of the crystals soaked in DMSO (DMSO@CCM-1, **Figure** 4a, blue line) for 24 h indicates that DMF is exchanged with the new solvent. Notably, the band corresponding to the DMF C=O stretching ($1654 \, cm^{-1}$) almost disappears after 24 h of soaking in DMSO. Instead, a strong band centered at $1006 \, cm^{-1}$ appears, corresponding to the S=O stretching of coordinated DMSO molecules which in neat DMSO is centered at $1043 \, cm^{-1}$.[34] Neat DMSO exhibits the S=O stretching at $1043 \, cm^{-1}$, which manifests itself as a shoulder to the $1006 \, cm^{-1}$ band, implying the presence of both metal-coordinated and noncoordinated DMSO within the exchanged MOF crystal. Additionally, the C—H stretching bands corresponding to the DMSO methyl groups appear at 3000 and $2915 \, cm^{-1}$ while those of DMF almost fully disappear. The material maintains a high degree of crystallinity after guest exchange as shown in Figure 4b (red trace). Additionally, the powder pattern of DMSO@CCM-1 is nearly identical to that of CCM-1 (Figure 4b, black trace), indicating that the framework does not undergo any significant structural changes upon the guest exchange.

The large channels or voids in MOFs can be utilized via SCSC transitions to encapsulate and structurally characterize clusters of guest molecules, including organic, inorganic, and gas
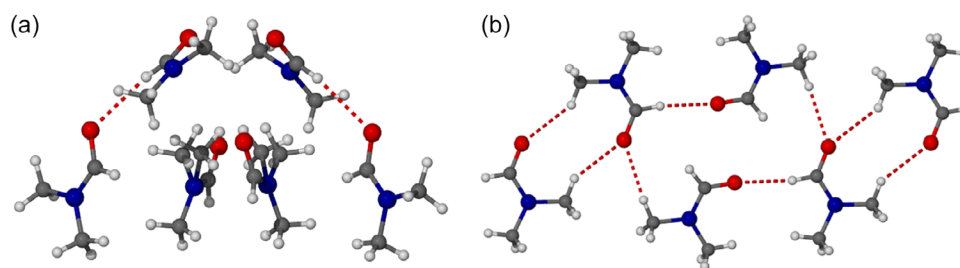
Figure 3. Single-crystal structures showing hydrogen bond interactions between DMF molecules in a) CCM-2 and b) bulk DMF. Hydrogen bonds are shown in red dashed lines. Gray: C. Red: O. Blue: N. White: H.

ADVANCED
SCIENCE NEWS
www.advancedsciencenews.com

small
structures
www.small-structures.com
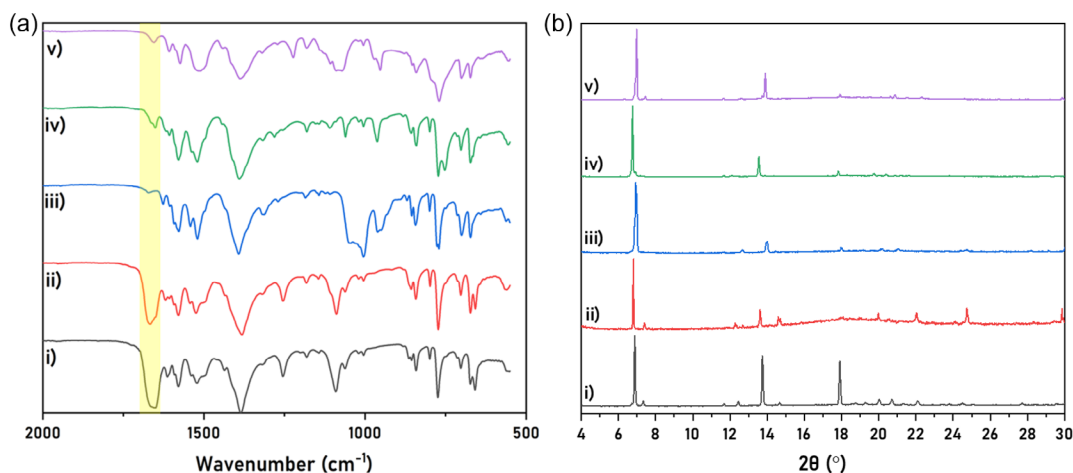
Figure 4. a) FT-IR spectra zoomed in to the 2000–500 cm^{-1} region of i) CCM-1, ii) CCM-2, iii) DMSO@CCM-1, iv) PYZ@CCM-1, and v) TAZ@CCM-1. b) PXRD patterns of i) CCM-1, ii) CCM-2, iii) DMSO@CCM-1, iv) PYZ@CCM-1, and v) TAZ@CCM-1. Yellow band on the FT-IR spectrum highlights the changes in the DMF C=O stretching upon guest inclusion.

molecules.[35] A landmark report by Yaghi and co-workers using MOF-303 containing 1-H-pyrazole-3,5-dicarboxylate linkers showed that the nucleation of water molecules can be visualized within the pores of the framework.[36] Combining synchrotron SC-XRD analysis with DFT calculations, the authors illustrated the nucleation and growth of water clusters containing up to 14 molecules. Additionally, Eddaoudi and co-workers were able to visualize a cluster of 114 water molecules sustained by hydrogen bonds within the cages of the Cr-**soc**-MOF.[16] By analyzing the structure of the discrete water cluster along with the accompanying adsorption isotherm, the authors were able to discern three water adsorption layers within the pores. Crucially, these results highlight that crystallographic analysis of MOF pore contents can yield both structural and mechanistic insights into the nucleation of molecules on the nanoscale.

SC-XRD analysis of DMSO@CCM-1, obtained by soaking single crystals of CCM-1 in DMSO, reveals the CCM-1 framework with encapsulated DMSO molecules yielding a structure with the formula La(BPDC)$_{1.5}$(DMSO)$_2$. **Figure 5**a shows the views along the b axis of the resulting MOF. Unlike the as-synthesized CCM-1, DMSO@CCM-1 contains two coordinated and two noncoordinated DMSO molecules inside the rhombic pores. While DMSO is ambivalent, it coordinates to the lanthanum(III) metal

center via the oxygen atom of the S=O moiety. This is expected due to lanthanum cations being hard acids and DMSO is known to coordinate to hard acids through the oxygen atoms and soft acids through the sulfur atom.[37,38] Two of the four DMSO molecules along the c axis were severely disordered and as a result were masked.[39] Overall, successful exchange of DMF with DMSO proves that CCM-1 is capable of guest exchange.

The bulk DMSO crystal structure was first solved in 1966 but was redetermined more precisely in 2017 by Reuter.[40,41] In the bulk, each DMSO molecule engages in four C—H...O hydrogen bonds with C···O distances ranging from 3.33 to 3.46 Å (Figure 5b). The molecules pack in a tube-like arrangement along the crystallographic b axis. This is significantly different from the packing of DMSO molecules inside CCM-1 which are arranged in a channel along the b axis. One C—H···O hydrogen bond between a methyl hydrogen atom of a coordinated DMSO and the oxygen atom of a noncoordinated has a length of 3.249(1) Å. There is a symmetry equivalent hydrogen bonding interaction inside the pore between the second pair of coordinated and noncoordinated DMSO molecules, resulting in two hydrogen bond interactions per pore. However, a hydrogen bonded tetramer does not form between these DMSO molecules. Further analysis about DMSO@CCM-1 is not possible due to high disorder.
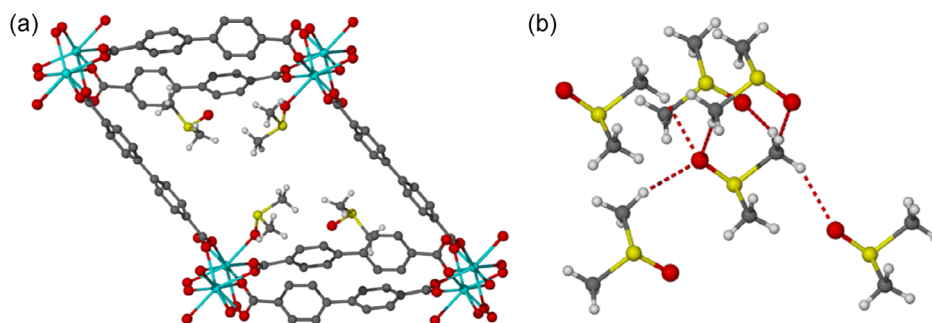
Figure 5. Single-crystal structures of a) DMSO@CCM-1 along the b axis and b) hydrogen bonding in bulk DMSO. Gray: C. Red: O. Yellow: S. White: H. Green: La. Hydrogen atoms of the CCM-1 framework omitted for clarity.

**ADVANCED
SCIENCE NEWS**

www.advancedsciencenews.com

**small
structures**

www.small-structures.com

As with DMF, the structure on included DMSO suggests an alternative packing arrangement in a potential alternative DMSO polymorph.

The capability of the CCM-series MOFs to undergo guest exchange as a single-crystal-to-single-crystal transition (SCSCT) was tested with a variety of nonsolvent liquid guests, a list of which is shown in Table S1, Supporting Information. The crystal quality of the immersed MOFs was first monitored visually using a polarizing microscope. If the crystals of the framework did not exhibit cracking or pseudomorphosis, a crystal was taken out of the guest liquid for FT-IR analysis. Most MOF crystals exhibit cracking within a few hours without showing full or even partial exchange. For MOF crystals immersed in 1-ethylpyrazole (EtPyz@CCM-1), 2,3-dihydrofuran (DHF@CCM-2), pyrimidine (PMD@CCM-2), 2-pyrrolidinone (2-PDN@CCM-2), 3-amino-pyrazole (AmPyz@CCM-2), SC-XRD confirmed partial exchange for all guest molecules, supported by FT-IR (Figure S6, Supporting Information), PXRD (Figure S7, Supporting Information) and NMR analysis (Figure S8–S12, Supporting Information). The high degree of crystallinity that is retained after soaking the MOF crystals in each of these guests is shown in their respective PXRD patterns in Figure S12, Supporting Information. Small changes in the peak positions of the PXRD patterns are due to the small changes that the MOF undergoes to accommodate guest molecules inside the pores. The stoichiometric ratio as revealed by SC-XRD for each material is $La(BPDC)_{1.5}(EtPyz)_1(DMF)_1$ $Eu(BPDC)_{1.5}(DHF)_2(DMF)_1$, $Eu(H_2BPDC)_{1.5}(PMD)_2(DMF)_1$, $Eu(H_2BPDC)_{1.5}(2\text{-}PDN)_{0.63}(DMF)_{1.37}$, and $Eu(BPDC)_{1.5}(3\text{-}AmPyz)_3$, respectively (Figure S13–S17, Supporting Information). Due to the partial exchange of these guest molecules, further discussion of the SC-XRD analysis of these materials will not be undertaken and the focus is on MOFs where the DMF solvent in the as-synthesized material is fully exchanged with the guest molecules.

Among such guests, pyridazine (PYZ) exhibited successful SCSCT with the FT-IR spectrum, indicating almost complete exchange of the guest (Figure 4a, green trace) as exemplified by a significant decrease in the intensity of the DMF C=O stretch at $1654\,\text{cm}^{-1}$ accompanied by the emergence of the PYZ C—H stretching mode at $3060\,\text{cm}^{-1}$ (full FT-IR spectra shown in Figure S4, Supporting Information). The exchange is further supported by the ^{1}H NMR spectrum of the dissolved crystals, which show the presence of both PYZ and a low intensity of DMF resonances (Figure S19, Supporting Information).

The SC-XRD structure of pyridazine-encapsulated CCM-1 (PYZ@CCM-1) is shown in **Figure 6** and yields an asymmetric unit with the formula $La_3(H_2BPDC)_{4.5}(PYZ)_9(DMF)$. The crystal structure of PYZ@CCM-1 contains two types of pores—those which are fully exchanged with pyridazine and those which are partially exchanged. The asymmetric unit contains nine PYZ molecules and one DMF solvent molecule while two-thirds of the pores are fully exchanged and one-third contains coordinated DMF molecules along with noncoordinated PYZ in a 1:2 ratio (DMF:PYZ, Figure 6). In the pores containing DMF, all four noncoordinated DMF molecules have been replaced with PYZ while the two coordinated DMF molecules remain. This suggests that it is the noncoordinated DMF molecules that can be exchanged first with PYZ. This phenomenon is also observed when CCM-2 is soaked in PMD. The coordinated DMF molecules remain in the MOF while noncoordinated solvent is exchanged with the guest molecules (Figure S17, Supporting Information). In the pores where PYZ coordinates to the framework metal centers, the guest molecule occupies both coordination centers. The La–N distance ranges from 2.634(6) to 2.679(6) Å for PYZ, slightly longer than the La–O distance of 2.543(6) Å for the coordinated DMF molecules. The slightly shorter, and likely stronger, coordination of DMF over pyridazine by the oxophilic metal center may explain why full exchange of the solvent with the guest was not achieved.

Given the ordered nature of the guests in PYZ@CCM-1, we were interested in whether confinement changes the packing arrangement of the encapsulated molecules as compared to the bulk. Three crystal structures at varying pressures of the same polymorph of neat pyridazine have been reported. The earliest was communicated by Blake and Rankin who obtained their sample by melting pyridazine and slowly cooling it to obtain a single crystal.[42] The other two structures were reported in 2010 by Katrusiak and co-workers, who published the crystal structures of PYZ at 0.27 and 0.61 GPa.[43] Despite the different conditions for all reported structures, the packing arrangement of PYZ molecules in the lattice does not change. PYZ stacks in nearly planar sheets and forms mainly C···N interactions. For the crystal structures collected at 0.27 and 0.61 GPa, the C···N distances range from 3.377(8) to 3.639(8) Å with respective angles ranging from 154 to 140°. In the bulk, each PYZ molecule participates in four C···N interactions with two neighboring PYZ molecules, averaging to two C···N interactions per nitrogen atom. Additionally, π–π interactions are present between PYZ
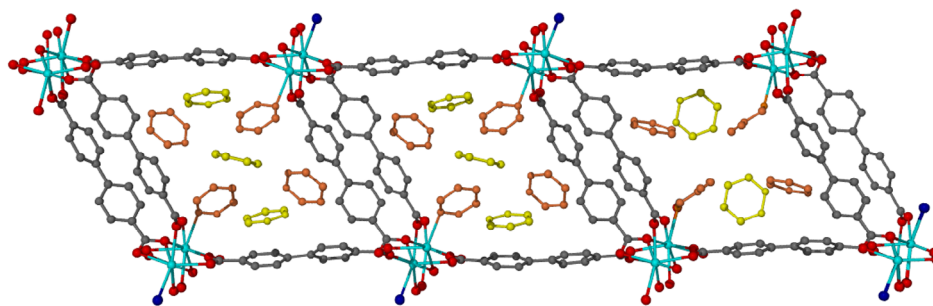
Figure 6. SC-XRD image of PYZ@CCM-1 along the *b* axis showing fully and partially exchanged pores. Gray: C. Dark blue: N. Red: O. Light blue: La. H atoms omitted for clarity.

**ADVANCED
SCIENCE NEWS**

www.advancedsciencenews.com

**small
structures**

www.small-structures.com

molecules of adjacent sheets. Meanwhile, there are no short N⋯N interactions as they are longer than those of C⋯N and π–π, indicating that the latter could play a more influential role in the nucleation and crystallization of PYZ.

Pyridazine molecules confined in CCM-1 form alternating clusters of trimers and tetramers resulting in an unusual seven-molecule repeating unit along the MOF channel along the *b* axis (Figure 6, yellow and orange molecules). This arrangement is significantly different from the bulk structure and represents a novel packing arrangement. This difference is naturally unsurprising given the coordinated nature of some of the PYZ molecules but highlights the ability of the MOF to profoundly influence the molecular aggregation. Indeed, seven-molecule repeat units are very uncommon in small molecular crystal structures as the most stable crystal structures are formed in systems with strong intermolecular interactions resulting in minimal free space and high symmetry.[44] Strikingly, however, these confined clusters of trimers and tetramers exhibit similar interactions to those in the bulk. For instance, the shortest interactions are those of C⋯N with a range of 3.319(12)–3.635(13) Å with respective angles ranging from 134 to 151°. Additionally, weak host–guest and guest–guest π–π interactions are present for the trimers which form a linear pentamer consisting of three PYZ units and two benzene units of the organic linker (Figure 6, yellow PYZ trimer and two benzene moieties facing the trimer edge PYZ molecules). Long host–guest π–π interactions with the distance of 4.029(8) and 4.169(7) Å are present between the edge PYZ molecules of the trimer and benzene units of the linkers, with interplanar angles of 12.4(8) and 12.9(6)°, respectively. The guest–guest π–π interactions have a distance of 4.284(9) and 4.095(6) Å, along with interplanar angles of 33.9(13) and 23.7(13)°, respectively, and complete the π–π pentamer.

In PYZ@CCM-1, the PYZ tetramer forms between two coordinated and two noncoordinated PYZ molecules. For the tetramer, there are no face-to-face interactions between the pyridazine molecules. This is likely to be due to the presence of coordination bonds between two of these pyridazine molecules and the lanthanum(III) metal centers, resulting in the guest molecules packing at an angle along the *b* axis pore. The two noncoordinated pyridazine molecules have the 1,2-nitrogen atoms pointing toward the center of the pore. Classical nucleation theory posits that the molecular packing inside nuclei of critical size reflects the lattice arrangement in the resulting polymorph.[45] Thus, this novel packing arrangement PYZ inside CCM-1 begins to suggest a model for an alternative bulk packing arrangement (**Figure 7**).

The SCSC guest exchange reaction was also attempted with 1,2,3-triazole (TAZ) by immersing single crystals of CCM-1 in the liquid guest at room temperature. After 24 h, the FT-IR spectrum of TAZ-soaked CCM-1 exhibits a significant decrease in the intensity of the C=O stretching band corresponding to the included DMF (Figure 4a, purple line). This band is replaced with broad peaks in the 2500–3500 cm⁻¹ range, characteristic of N–H (3133 cm⁻¹) and C–H (3006 cm⁻¹) stretches of TAZ. In the pure TAZ spectrum, the peaks at 1068, 1091, and 1113 cm⁻¹ were assigned to two δ(CH) and one δ(NH) (in-plane bending) modes, respectively.[46] The peak assigned to the N=N stretching in pure TAZ at 1514 cm⁻¹ exhibits a widening and shifts to 1524 cm⁻¹ in TAZ@CCM-1, indicative of a coordination bond forming between the aromatic nitrogen atom and lanthanum metal center. The exchange of DMF with TAZ is further corroborated by the ¹H NMR spectrum of the dissolved MOF which shows the presence of the protons of the TAZ ring at 7.86 ppm (Figure S11, Supporting Information). The PXRD pattern of TAZ-soaked crystals of CCM-1 (Figure 4b, purple line) exhibits high crystallinity and consequently the crystals were analyzed by SC-XRD. The resulting crystal structure shows that TAZ has fully exchanged with DMF, yielding TAZ@CCM-1 with a formula of La(BPDC)$_{1.5}$(TAZ)$_4$ containing four TAZ molecules in the asymmetric unit and resulting in the formation of octamers along the crystallographic *b* axis (**Figure 8**a,b). Of the four unique TAZ molecules, two are identified as 1H-TAZ and the two others as 2H-TAZ tautomers, resulting in tautomeric isomorphism.[47] While isomorphism is less common, tautomeric polymorphism is relatively common with 51% of crystal structures reported in the CSD being capable of containing more than one tautomeric form.[48] The N–N–N angles of the 1H-TAZ molecules are 103(2)° and 107.4(8)° and those of 2H-TAZ molecules are 109.5(14)° and 107.9(6)°. In bulk TAZ, the N–N–N angle is 115.9(3)° for 2H-TAZ and 106.5(2)° for 1H-TAZ.[47] The larger N–N–N angle of the encapsulated 2H-TAZ molecules supports the tautomer assignment. CCM-1 undergoes some structural
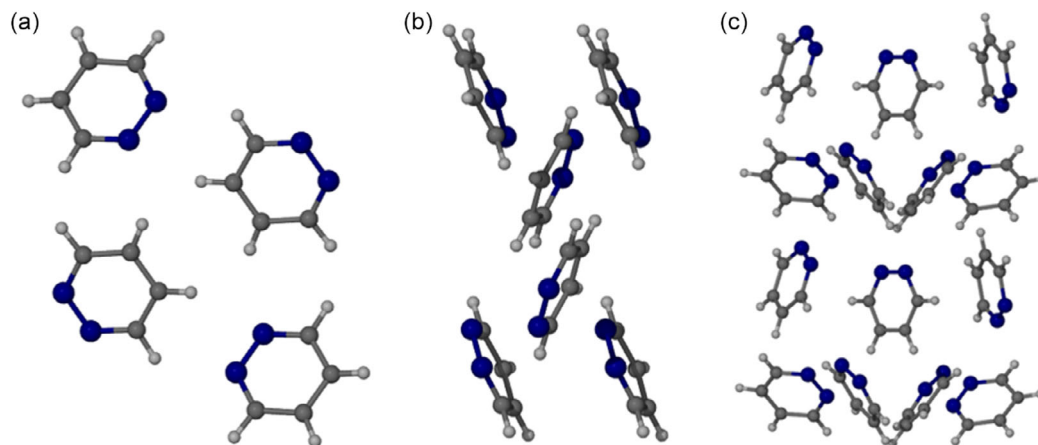
Figure 7. Unit cell of bulk pyridazine along the a) *a* and b) *c* axes. c) Pyridazine trimer and tetramer clusters inside PYZ@CCM-1. Gray: C. Blue: N. White: H.
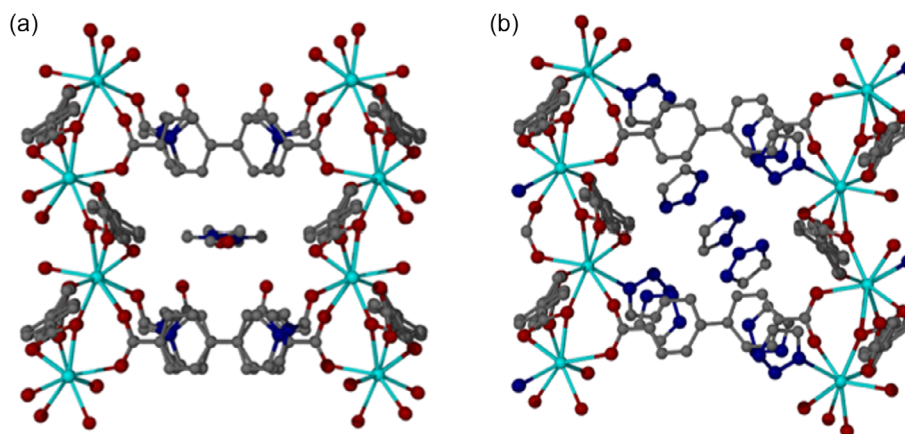
Figure 8. Single-crystal structures along the crystallographic *a* axis of a) CCM-1 and b) TAZ@CCM-1. Gray: C. Red: O. Dark blue: N. Light blue: La. Hydrogen atoms omitted for clarity.

changes to accommodate TAZ inside the pores including a phase change to the centrosymmetric $P2_1/n$, as opposed to the chiral *C*2 of as-synthesized CCM-1. Along the *b* axis, both frameworks look similar, but significant changes are observed along the *a* axis. Along the *a* axis of CCM-1, the SBUs and organic linkers are parallel to one another while in TAZ@CCM-1 they appear to shift down so that all TAZ molecules can occupy the pores. The encapsulation of TAZ molecules in CCM-3 (TAZ@CCM-3) MOF was also attempted. Crucially, in CCM-3, an identical molecular cluster of TAZ as that in CCM-1 forms, suggesting that the molecular clusters do not form randomly in these MOFs, but indeed the assembly is guided by confinement and intermolecular interactions.

The structure of the encapsulated TAZ molecules shows that there are stabilizing intermolecular hydrogen bonds and π–π interactions. The hydrogen bonding network starts from the coordinated TAZ molecule (T1, **Figure 9**a), which participates in two hydrogen bonding interactions with neighboring TAZ molecules (T2 and T3) acting as both the donor and acceptor. The hydrogen bond between T1 and T3 exhibits a N1···N3 distance of 3.071(11) Å along with an angle of 167.0(3)°. The other hydrogen bond N2···N1 exhibits an N···N distance of 2.799(10) Å and an angle of 161.1(4)°. Both T2 and T3 subsequently interact with T4 through two hydrogen bonds, forming a hydrogen bonded tetramer. This tetramer subsequently grows into a hexamer by the addition of T5 and T6 by both hydrogen bonding and π–π interactions with T2 and T3. Finally, the octamer is completed by the addition of terminal T7 and T8, both of which hydrogen bond strictly with T5 and T6. The π–π interactions between T3 and T5 along with T2 and T6 are symmetry equivalent and both have a distance of 3.45(1) Å.

There is a π–π interaction with a distance of 4.149(15) Å between both T7 and T8 with neighboring aromatic moieties of the organic linker. This is a relatively long hydrophobic interaction when comparing to the π–π interactions between the guest–guest TAZ units. Additionally, C—H···N hydrogen bonding interactions with C···N distances ranging between 3.594(8) and 3.791(18) Å are also present. Consequently, these host–guest interactions may act as additional stabilizing interactions toward
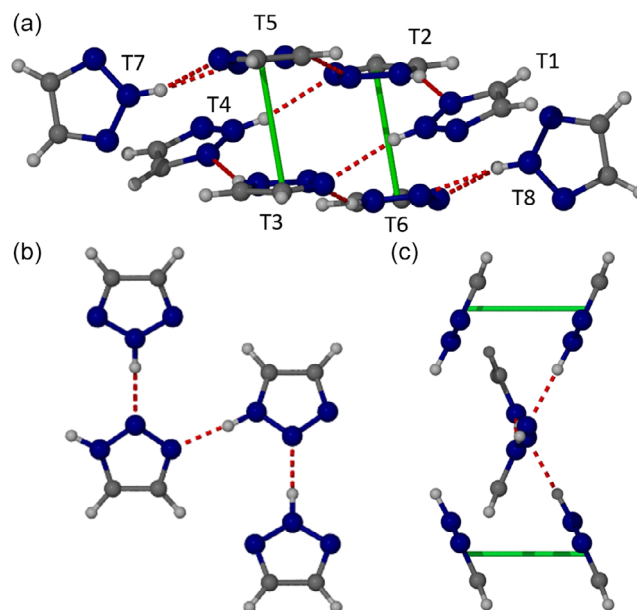
Figure 9. SC-XRD structures of a) the TAZ octamer in TAZ@CCM-1 while b) and c) show the bulk arrangement of TAZ. Hydrogen bonds and π–π interactions are shown as red dashed and green solid lines, respectively. Gray: C. Blue: N. White: H.

the TAZ cluster, but the arrangement of TAZ molecules within the framework is mainly guided by guest–guest interactions.

In the bulk, neat TAZ crystallizes as a 1:1 molecular complex of its two tautomers, 1H-1,2,3-triazole (1H-TAZ) and 2H-1,2,3-triazole (2H-TAZ) as in the CCM included guests.[49] Apart from containing the pyrrolic hydrogen atom in either 1H or 2H positions, the two tautomers also differ by their ring angles. Both tautomers pack in a herringbone arrangement with adjacent rings having a dihedral angle of 49(1)°. The shortest intermolecular interaction is the N—H···N hydrogen bond between two adjacent 1H-TAZ molecules with 2.779(2) Å (Figure 9b, hydrogen bond between two 1H-TAZ molecules). The second shortest intermolecular interaction is between two adjacent 1H-TAZ

2400300 (8 of 10)

and 2H-TAZ molecules with the N—H···N hydrogen bond having the distance of 2.935(3) Å. Additional π–π interactions between adjacent 1H-TAZ molecules with the length of 3.7 Å further act to stabilize the crystal lattice.

Crucially, both hydrogen bonding and π–π interactions are present in both the bulk and confined clusters. Additionally, the ratio of 1H- and 2H-TAZ in both bulk and confined clusters is 1:1. The most significant difference between these bulk and confined clusters is their shape and size. While in both bulk and confined crystal structures the main stabilizing forces are hydrogen bonds and π–π interactions, in CCM-1 the cluster shape is also guided by the external framework. Thus, it is encouraging to observe that the same intermolecular interactions guide the formation of an octanuclear cluster of TAZ with a unique shape, which suggests that it could be potentially used to unveil novel polymorphs. Additionally, an identical cluster of TAZ molecules forms inside the pores of CCM-3, indicating that this cluster represents a stable structure, as opposed to one that forms randomly, within the MOF.

3. Conclusion

In conclusion, lanthanoid-based MOFs CCM-1–4 have been used to describe the formation of molecular clusters inside the framework channels. While partially exchanged systems could not be compared to their bulk equivalents, they potentially highlight the mechanism of guest exchange, based on the oxophilicity of the guest molecule. The arrangement of TAZ clusters in CCM-1 significantly differs from that of the bulk material. Under confinement in the CCM-1 MOF, it seems like the generally weaker hydrophobic interactions guide the formation of clusters while in bulk the directionality is gained from hydrogen bonds resulting in herringbone-style packing. Finally, while the environment within the present MOFs is of course very different to the bulk guests and the cavity size is relatively small compared to the size of a critical nucleus, these initial results nevertheless show that clusters of significant size and very different packing arrangements to the bulk guests can be generated by confinement. This kind of approach represents a possible step along the pathway to stabilizing hitherto unobserved polymorphs, particularly those calculated by CSP approaches,[49,50] and shedding light on molecular clusters of subcritical size. Confining the molecular cluster in a matrix which has controllable shape and size can lead to the formation of oligomers exhibiting novel shapes and sizes.

4. Experimental Section

^{1}H NMR (400 MHz, DMSO-d_6, δ): 7.15 (s, 2H, Ar H), 1.30 (q, $J = 8$ Hz, 2H; CH$_2$), 0.90 (t, $J = 8$ Hz, 3H; CH$_3$); {^{1}H}^{13}C NMR (100 MHz, CDCl$_3$, δ): 175.4 (C=O), 156.5 (C4); IR (KBr): $\nu = 2972$ (w), 2907 (w), ..., 1026 (s; ν_{as}(SiOSi)), 971 (ν_s), ..., 666 (w; ν_s(SiOSi)), ..., 439 (m), 401 cm^{-1} (m); UV–vis (n-hexane): λ_{max} (ε) = 320 (5000), 270 nm (12 000); EIMS m/z (%): 108 (20) [M$^+$], 107 (60) [M$^+$ − H], 91 (100) [C$_7$H$_7^+$]; HRMS (ESI) m/z: [M + H]$^+$ calc. for C$_{21}$H$_{38}$N$_4$O$_6$S, 475.2591; found, 475.2593. Anal. calc. for C$_{45}$H$_{28}$N$_4$O$_7$: C 62.47, H 3.41, N 6.78; found: C 62.27, H 3.46, N 6.80.

General Synthesis Method:: All MOFs discussed herein were synthesized by similar synthetic procedures. In a vial, a lanthanum salt (0.14 mmol) was mixed together with 7 mL of DMF. A supersaturated stock solution of the organic linker, H$_2$BPDC, with the concentration of 41.3 mM was prepared and 5.04 mL of it was added to the metal salt solution. Prior to the addition of the organic linker, the stock solution was heated to ensure full dissolution of the linker. After the two solutions had been combined, the resulting mixture was sonicated for 5–10 min. In the case of CCM-1, 0.21 mL of TFA was added to the mixture prior to the sonication step. After sonication, the mixture was transferred into a Teflon-lined acid digestion vessel which was placed in an isothermal oven at 120 °C for 72 h and was cooled to room temperature over the course of 6 h. After this, the acid digestion vessel was removed from the oven and single crystals with a plank shape were observed at the bottom of the vessel. After decanting the mother liquor, the crystals were carefully removed and placed in fresh DMF where the crystallinity could be retained for months.

CCM-1: The compound was obtained as transparent plank-shaped single crystals (55 mg, 55% based on crystallographic formula). ^{1}H NMR (400 MHz, DMSO–d_6, δ): 7.83–7.86 (4H, $J = 8.6$ Hz, dt, Ar–H), 8.01–8.04 (4H, $J = 8.6$ Hz, dt, Ar–H); {^{1}H}^{13}C NMR (100.6 MHz, DMSO–d_6, δ): 127.62, 130.48, 130.79, 143.54, 167.46; IR (KBr): $\nu = 2929$ (m; C—H), 2864 (m; C—H), 1654 (s; C=O); Anal. calc. for C$_{21}$H$_{12}$O$_6$La(H$_2$O)$_3$(C$_3$H$_7$NO)$_3$: C 46.64, H 5.09, N 5.44; found: C 46.47, H 4.97, N 5.72. The formula determined from elemental analysis contains three additional water molecules and one fewer DMF molecule compared to the crystallographic formula.

CCM-2: Compound was obtained as transparent plank-shaped single crystals that show pink luminescence under UV light (48 mg, 47% based on crystallographic formula). ^{1}H NMR (400 MHz, DMSO–d_6, δ): 7.84–7.86 (4H, $J = 8.6$ Hz, dt, Ar–H), 8.01–8.04 (4H, $J = 8.6$ Hz, dt, Ar–H); {^{1}H}^{13}C NMR (100.6 MHz, DMSO–d_6, δ): 127.63, 130.49, 130.79, 143.54, 167.46; IR (KBr) $\nu = 2930$ (m; C—H), 2858 (m; C—H), 1655 (s; C=O); Anal. calc. for C$_{21}$H$_{12}$O$_6$Eu(H$_2$O)(C$_3$H$_7$NO): C 47.77, H 3.51, N 2.32, found: C 47.90, H 3.09, N 2.29. The formula determined from elemental analysis contains one more water molecule and three fewer DMF molecules compared to the crystallographic formula.

CCM-3: Compound was obtained as light green plank-shaped single crystals (50 mg, 50% based on crystallographic formula). ^{1}H NMR (400 MHz, DMSO–d_6, δ): 7.83–7.85 (4H, $J = 8.6$ Hz, dt, Ar–H), 8.01–8.03 (4H, $J = 8.6$ Hz, dt, Ar–H); {^{1}H}^{13}C NMR (100.6 MHz, DMSO–d_6, δ): 127.63, 130.49, 130.78, 143.54, 167.47; IR (KBr) $\nu = 2930$ (m; C—H), 2862 (m; C—H), 1655 (s; C=O); Anal. calc. for C$_{21}$H$_{12}$O$_6$Ce(H$_2$O)(C$_3$H$_7$NO)$_2$: C 48.79, H 4.25, N 4.21, found: C 48.70, H 3.69, N 4.25. The formula determined from elemental analysis contains one more water molecule and two fewer DMF molecules compared to the crystallographic formula.

CCM-4: Compound was obtained as dark green plank-shaped single crystals (43 mg, 43% based on crystallographic formula). ^{1}H NMR (400 MHz, DMSO–d_6, δ): 7.82–7.85 (4H, $J = 8.6$ Hz, dt, Ar–H), 8.00–8.03 (4H, $J = 8.6$ Hz, dt, Ar–H); {^{1}H}^{13}C NMR (100.6 MHz, DMSO–d_6, δ): 127.63, 130.49, 130.77, 143.53, 167.47; IR (KBr) $\nu = 2929$ (m; C—H), 2857 (m; C—H), 1663 (s; C=O); Anal. calc. for C$_{21}$H$_{12}$O$_6$Pr(C$_3$H$_7$NO): C 50.19, H 3.33, N 2.44, found: C 49.97, H 3.10, N 2.41. The formula determined from elemental analysis contains three fewer DMF molecules compared to the crystallographic formula.

[CCDC 2361696-2361708 contains the supplementary crystallographic data for this paper. These data can be obtained free of charge from The Cambridge Crystallographic Data Centre via www.ccdc.cam.ac.UK/data_request/cif].

Supporting Information

Supporting Information is available from the Wiley Online Library or from the author.

Conflict of Interest

The authors declare no conflict of interest.

Author Contributions

Jonathan W. Steed: Conceptualization (lead); Formal analysis (equal); Funding acquisition (lead); Investigation (equal); Project administration (lead); Supervision (lead); Writing—original draft (equal); Writing—review and editing (equal). **Alan Braschinsky**: Formal analysis (lead); Investigation (lead); Methodology (equal); Writing—original draft (equal). **Toby J. Blundell**: Data curation (equal); Formal analysis (equal); Writing—review and editing (supporting).

Data Availability Statement

Keywords

[1] P. G. Vekilov, *Nanoscale* **2010**, *2*, 2346.
[2] P. G. Vekilov, *Nature* **2019**, *570*, 450.
[3] J. Li, F. L. Deepak, *Chem. Rev.* **2022**, *122*, 16911.
[4] N. E. Levinger, *Science* **2002**, *298*, 1722.
[5] M. Alcoutlabi, G. B. Mckenna, *J. Phys: Condens. Matter* **2005**, *17*, R461.
[6] M. Juramy, R. Chèvre, P. C. Vioglio, F. Ziarelli, E. Besson, S. Gastaldi, S. Viel, P. Thureau, K. D. M. Harris, G. Mollica, *J. Am. Chem. Soc.* **2021**, *143*, 6095.
[7] R. Kubota, S. Tashiro, M. Shiro, M. Shionoya, *Nat. Chem.* **2014**, *6*, 913.
[8] M. Kawano, M. Fujita, *Coord. Chem. Rev.* 251, 2592.
[9] E. Fernandez-Bartolome, A. Martinez-Martinez, E. Resines-Urien, L. Piñeiro-Lopez, J.S. Costa, *Coord. Chem. Rev.* 452, 214281.
[10] M. I. Gonzalez, A. B. Turkiewicz, L. E. Darago, J. Oktawiec, K. Bustillo, F. Grandjean, G. J. Long, J. R. Long, *Nature* **2020**, *577*, 64.
[11] J.P. Zhang, P.Q. Liao, H.L. Zhou, R.B. Lin, X.M. Chen, *Chem. Soc. Rev.* **2014**, *43*, 5789.
[12] E. Chaudhary, A. Mohammad, S. Mobin, *Cryst. Growth Des.* **2017**, *17*, 2893.
[13] Y. Inokuma, S. Yoshioka, J. Ariyoshi, T. Arai, Y. Hitora, K. Takada, S. Matsunaga, K. Rissanen, M. Fujita, *Nature* **2013**, *495*, 461.
[14] M. Hoshino, A. Khutia, H. Xing, Y. Inokuma, M. Fujita, *IUCrJ* **2016**, *3*, 139.
[15] L. M. Hayes, C. E. Knapp, K. Y. Nathoo, N. J. Press, D. A. Tocher, C. J. Carmalt, *Cryst. Growth Des.* **2016**, *16*, 3465.
[16] S. M. Towsif Abtab, D. Alezi, P. M. Bhatt, A. Shkurenko, Y. Belmabkhout, H. Aggarwal, Ł. J. Weseliński, N. Alsadun, U. Samin, M. N. Hedhili, M. Eddaoudi, *Chem* **2018**, *4*, 94.
[17] J. Liu, C. E. Nicholson, S. J. Cooper, *Langmuir* **2007**, *23*, 7286.
[18] S. D. Durbin, G. Feher, *Annu. Rev. Phys. Chem.* **1996**, *47*, 171.
[19] Y. F. Han, X. H. Zhou, Y. X. Zheng, Z. Shen, Y. Song, X. Z. You, *CrystEngComm* **2008**, *10*, 1237.
[20] R. Łyszczek, L. Mazur, *Centr. Eur. J. Chem.* **2012**, *10*, 1165.
[21] J. Lee, N. W. Waggoner, L. Polanco, G. R. You, V. M. Lynch, S. K. Kim, S. M. Humphrey, J. L. Sessler, *Chem. Commun.* **2016**, *52*, 8514.
[22] A. J. R. Thom, E. Regincós Martí, I. Pakamorė, C. Wilson, R. S. Forgan, *Z. Anorg. Allg. Chem.* **2022**, *648*, 1.
[23] G. B. Deacon, R. J. Phillips, *Coord. Chem. Rev.* **1980**, *33*, 227.
[24] W. Gong, Z. Chen, J. Dong, Y. Liu, Y. Cui, *Chem. Rev.* **2021**, *122*, 9078.
[25] F. Saraci, V. Quezada-Novoa, P. R. Donnarumma, A. J. Howarth, *Chem. Soc. Rev.* **2020**, *49*, 7949.
[26] A. Schoedel, M. Li, D. Li, M. O'Keeffe, O. M. Yaghi, *Chem. Rev.* **2016**, *116*, 12466.
[27] C. F. MacRae, I. Sovago, S. J. Cottrell, P. T. A. Galek, P. McCabe, E. Pidcock, M. Platings, G. P. Shields, J. S. Stevens, M. Towler, P. A. Wood, *J. Appl. Crystallogr.* **2020**, *53*, 226.
[28] K. Binnemans, C. Görrler-Walrand, *Chem. Phys. Lett.* **1995**, *235*, 163.
[29] M. Rahm, R. Hoffmann, N. W. Ashcroft, *Chem. Eur. J.* **2016**, *22*, 14625.
[30] V. A. Blatov, A. P. Shevchenko, D. M. Proserpio, *Cryst. Growth Des.* **2014**, *14*, 3576.
[31] C. R. Groom, I. J. Bruno, M. P. Lightfoot, S. C. Ward, *Acta Crystallogr. Sect. B: Struct. Sci. Cryst. Eng. Mater.* **2016**, *72*, 171.
[32] H. Borrmann, I. Persson, M. Sandström, C. M. V Stålhandske, *J. Chem. Soc. Perkin Trans.* **2000**, *2*, 393.
[33] M. B. Majewski, A. J. Howarth, P. Li, M. R. Wasielewski, J. T. Hupp, O. K. Farha, *CrystEngComm* **2017**, *19*, 4082.
[34] J.-C. G. Bünzli, J.-P. Metabanzoulou, P. Froidevaux, L. Jin, *Inorg. Chem* **1990**, *29*, 3875.
[35] A. Braschinsky, J.W. Steed, *Coord. Chem. Rev.* **2022**, *473*, 214840.
[36] N. Hanikel, X. Pei, S. Chheda, H. Lyu, W. Jeong, J. Sauer, L. Gagliardi, O.M. Yaghi, *Science* **2021**, *374*, 454.
[37] G. Kastner, H. Reuter, *Main Group Met. Chem.* **1999**, *22*, 605.
[38] F. D. Rochon, R. Melanson, *Can. J. Chem.* **1975**, *53*, 2371.
[39] A. L. Spek, *Acta Crystallogr.. Sect. C: Struct. Chem.* **2015**, *71*, 9.
[40] R. Thomas, C. Brink Shoemaker, K. Eriks, *Acta Cryst.* **1966**, *21*, 12.
[41] H. Reuter, *Acta Crystallogr. Sect. E: Crystallogr. Commun.* **2017**, *73*, 1405.
[42] A. J. Blake, D. W. H. Rankin, *Acta Cryst.* **1991**, *C47*, 1933.
[43] M. Podsiadlo, K. Jakobek, A. Katrusiak, *CrystEngComm* **2010**, *12*, 2561.
[44] K. M. Steed, J. W. Steed, *Chem. Rev.* **2015**, *115*, 2895.
[45] R. J. Davey, S. L. M. Schroeder, J. H. Ter Horst, *Angew. Chem. Int. Ed.* **2013**, *52*, 2166.
[46] B. E. Borello, A. Zecchina, E. Guglielminotti, *J. Chem. Soc. B* **1969**, *8*, 307.
[47] R. Goddard, O. Heinemann, C. Krüger, *Acta Cryst.* **1997**, *C53*, 1846.
[48] A. Woods-Ryan, C. L. Doherty, A. J. Cruz-Cabeza, *CrystEngComm* **2023**, *25*, 2845.
[49] A. R. Oganov, C. J. Pickard, Q. Zhu, R. J. Needs, *Nat. Rev. Mater.* **2019**, *4*, 331.
[50] J. E. Carpenter, M. Grünwald, *J. Am. Chem. Soc.* **2021**, *143*, 21580.